Sustainable Energy & Fuels

# Comparative study of undoped, boron-doped, and boron/fluorine dual-doped carbon nanoparticles via solution plasma as catalysts for the oxygen reduction reaction

| | |
|---|---|
| Journal: | *Sustainable Energy & Fuels* |
| Manuscript ID | SE-ART-05-2020-000708.R1 |
| Article Type: | Paper |
| Date Submitted by the Author: | 15-Jun-2020 |
| Complete List of Authors: | Chokradjaroen, Chayanaphat; Shibaura Institute of Technology, SIT Research Laboratories,<br>Kato, Shuhei; Shibaura Institute of Technology, Materials Science and Engineering, Graduate School of Engineering and Science<br>Fujiwara, Kensuke; Shibaura Institute of Technology, Materials Science and Engineering, Graduate School of Engineering and Science<br>Watanabe, Hiroko; Shibaura Institute of Technology, Materials Science and Engineering, Graduate School of Engineering and Science<br>Ishii, Takahiro; Shibaura Institute of Technology, Materials Science and Engineering, Graduate School of Engineering and Science<br>Ishizaki, Takahiro; Shibaura Institute of Technology, Department of Materials Science and Engineering, Faculty of Engineering, |
| | |

ARTICLE

# Comparative study of undoped, boron-doped, and boron/fluorine dual-doped carbon nanoparticles via solution plasma as catalysts for the oxygen reduction reaction

Received 00th January 20xx,
Accepted 00th January 20xx

DOI: 10.1039/x0xx00000x

Chayanaphat Chokradjaroen,[a] Shuhei Kato,[b] Kensuke Fujiwara,[b] Hiroko Watanabe,[b] Takahiro Ishii,[b] and Takahiro Ishizaki*[,b,c]

Boron/fluorine dual-doped carbons, which have never been reported for their oxygen reduction reaction (ORR) activity, were successfully synthesized through one-step solution plasma (SP) using mixtures of toluene, as a source of carbon, and heterocyclic compounds containing boron and fluorine atoms, i.e., 2,4,6-tris(4-fluorophenyl)boroxin, 2,4,6-tris(3,4-difluorophenyl)boroxin and 2,4,6-tris(3,4,5-trifluorophenyl) boroxin. Therefore, in this study, the obtained undoped, boron-doped, and boron/fluorine dual-doped carbons, synthesized by SP, were investigated and compared to find the catalytic activity toward ORR. FE-SEM observation exhibited that the obtained carbons had a diameter in the nanoscale range. XRD and Raman measurements revealed that the synthesis via SP led to the generation of turbostratic carbons with structural defect sites. The carbon atoms were found to mainly link with fluorine atoms through semi-ionic C-F bonding. All SP-synthesized carbon nanoparticles revealed the acceptable ORR activity in alkaline solution. However, boron/fluorine dual-doped carbon nanoparticles also showed the ORR through a two-electron pathway with the low generation of the unstable peroxide, $HO_2^-$, compared to undoped and boron-doped carbon nanoparticles.

## 1. Introduction

Consumption of fossil fuels is driving a climate crisis across the world. Therefore, the invention of alternative technologies, that can efficiently and environmental-friendly generate electricity from renewable sources, has gathered attention. Fuel cell is one of the promising technologies that show high potential for substituting conventional combustion-based power generating technologies, as well as, reducing emissions of pollutants such as greenhouse gases.[1] Fuel cells are generally composed of anode and cathode. In a fuel cell, fuels, such as $H_2$ molecules, are oxidized on the anode and the released electrons flow through the external circuit to the cathode where $O_2$ molecules are reduced.[1] Oxygen reduction reaction (ORR) is considered as the rate-limiting step in the fuel cells, such as proton exchange membrane fuel cells (PEMFCs).[2] Hence, the cathode usually contributes toward the electrochemical kinetic and system cost. ORR usually required expensive Pt-based catalysts.[3] In order to replace commercial Pt-based catalysts and find more cost-effective catalysts with good electrocatalytic activity, long-term cycling stability, and oxidation tolerance, several materials have been studied and proposed.[1, 4, 5] Metal-free heteroatom-doped carbon has been one of the most rapidly developed catalysts in the last decades, as giving examples in **Table 1**. Introduction of heteroatoms into graphitic carbon frameworks was reported that it could distribute and lead to asymmetry of spin and charge densities.[5, 6] This distribution can be considered as a key factor for tailoring the electronic arrangement, resulting in the enhancement of ORR activity of carbon.[5, 7] In comparison with Pt-based carbon catalysts, metal-free heteroatom-doped carbon also revealed the superior long-term durability and tolerance to metal oxidation.[7-9] Even though the ORR activity of metal-free heteroatom-doped carbon is still lower than that of the Pt-based carbon catalysts, the further development, such as dual or multi-doping of heteroatoms,[10, 11] may lead to more efficient ORR catalysts for energy conversion.

Boron-doped carbon materials have been widely studied for improving the ORR activity of carbon materials.[12] For example, in boron-doped carbon nanotubes, the vacant $2p^2$ orbital of boron conjugates with the carbon $\pi$ system to extract electrons, due to lower electronegativity of boron than carbon, leading to the electropositive boron sites, where $O_2$ molecules can be adsorbed and reduced.[13] Moreover, fluorine-doped carbons have recently been reported for their enhancement of ORR activity, compared to carbon alone.[7, 14] Since fluorine is an element with the largest electronegativity, it should be able to delocalize charges in the carbon framework, resulting in altering the charge distributions and facilitating $O_2$ adsorption.[15] Therefore, the additional doping of fluorine into boron-doped carbon was expected to improve the ORR activity.

Metal-free heteroatom-doped carbons, such as boron-doped and fluorine-doped carbons, can be synthesized by several strategies, for instance, chemical vapor deposition and pyrolysis

[a] SIT Research Laboratories, Shibaura Institute of Technology, Tokyo, 135-8548, Japan.
[b] Materials Science and Engineering, Graduate School of Engineering and Science, Shibaura Institute of Technology, Tokyo, 135-8548, Japan.
[c] Department of Materials Science and Engineering, College of Engineering, Shibaura Institute of Technology, Tokyo, 135-8548, Japan.
* Corresponding Author (ishizaki@sic.shibaura-it.ac.jp)
Electronic Supplementary Information (ESI) available, DOI: 10.1039/x0xx00000x

(**Table 1**). So far, these strategies usually require high temperatures, specific catalysts, inert gases, and multi-step synthesis. Recently, liquid-phase plasma technology, so-called solution plasma (SP), has been reported that it can simply synthesize carbon doped with heteroatoms under mild conditions, i.e., relatively low temperature and atmospheric pressure.[18] SP can be generated between electrodes by using a bipolar-pulsed power supply. Electricity flows to the tips of electrodes, which are submerged in a solution, and some molecules, e.g., $H_2O$ and benzene, nearby the electrodes are continuously collided by the electrons coming out from the electrodes, leading to the formation of highly active species (e.g., $H_2O \rightarrow \bullet H, \bullet OH, H^+, OH^-$ and $C_6H_6 \rightarrow \bullet H, H^+, \bullet C_2$).[18-20] These highly active species can further interact with other molecules in the solution and then chemical reactions occur rapidly. The formation of a variety of highly active species depends on molecules existing in a solution. Therefore, the synthesis of several heteroatom-doped carbon nanoparticles from many organic solvents (e.g., pyrrole ($C_4H_5N$) and triphenyl borate ($C_{18}H_{15}BO_3$)) using SP could be conducted and reported.[8, 19] According to this strategy, carbon nanoparticles with dual-doping of boron and fluorine atoms were expected to be simultaneously synthesized by SP under the organic solutions containing boron and fluorine.

In this study, boron/ fluorine dual-doped carbon nanoparticles were synthesized, for the first time, in comparison with undoped and boron-doped carbon nanoparticles. The undoped and boron-doped carbon nanoparticles were synthesized from toluene alone and a mixture of toluene and boron-containing solvent (i.e., 2,4,6-triphenylboroxin), respectively, and boron/fluorine dual-doped carbon nanoparticles were synthesized by using toluene mixed with solvents containing both boron and fluorine atoms (i.e., 2,4,6-tris(4-fluorophenyl) boroxin, 2,4,6-tris(3,4-difluorophenyl)boroxin and 2,4,6-tris(3,4,5-tri fluorophenyl)boroxin). The synthesis was conducted in one step at room temperature and atmospheric pressure without the addition of other chemicals. The characterization of the obtained undoped, boron-doped, and dual boron/fluorine-doped carbon nanoparticles was conducted for comparative study by using field emission scanning electron microscopy (FE-SEM), X-ray diffraction (XRD), Raman spectroscopy, X-ray photoelectron spectroscopy (XPS), and elemental analysis. The influence of the boron and fluorine dopants on morphological, structural, and chemical properties was investigated. Finally, electrocatalytic activity for ORR of all obtained products was evaluated.

## 2. Experimental

### 2.1 Materials

Toluene ($C_6H_5CH_3$, purity 99.5%), ethanol ($C_2H_5OH$, purity 99.5%), and 0.1 M potassium hydroxide (KOH) aqueous solution were purchased from Kanto Chemical Co., Inc. 2,4,6-Triphenylboroxin, TPBO ($C_{18}H_{15}B_3O_3$, purity >98.0%), 2,4,6-Tris(4-fluorophenyl)boroxin, TFPB ($C_{18}H_{12}B_3F_3O_3$, purity >98.0%), 2,4,6-Tris(3,4-difluorophenyl) boroxin, TDFPB ($C_{18}H_9B_3F_6O_3$, purity >98.0%) and 2,4,6-Tris(3,4,5-trifluorophenyl)boroxin, TTFPB ($C_{18}H_6B_3F_9O_3$, purity >98.0%) were purchased from Tokyo Chemical Industry Co., Ltd. Nafion® solution (5 wt% in a mixture of lower aliphatic alcohols and water) was purchased from Sigma-Aldrich. Ultrapure water (18.2 MΩ cm) was obtained from a RFD250NB Aquarius water purification system. All reagents were analytical grade and used without further purification.

### 2.2 Synthesis of boron/fluorine dual-doped carbon nanoparticles

TPBO, TFPB, TDFPB, and TTFPB were used as boron and fluorine sources, while toluene was used as a carbon source. TPBO, TFPB, TDFPB, and TTFPB were firstly added to 100 mL of toluene to make a final concentration of 10 mM and then kept stirring for 10 min. After

**Table 1** Examples of carbon-supported Pt and metal-free heteroatom-doped carbon materials and their properties (Note: SP and CVD refer to solution plasma and chemical vapor deposition, respectively. Pt, N, F and B refer to platinum, nitrogen, and boron, respectively.)

| Methods | Electrocatalysts | Electrocatalytic performance | | | Ref. |
|---|---|---|---|---|---|
| | | Conditions | On-set potential (V) | Current density (mA $cm^{-2}$) | |
| Commercial | 20% Pt on carbon Vulcan XC-72 (0.2 $mg_{cat}$ $cm^{-2}$) | 0.1M KOH (at 10 $mVs^{-1}$and 1600 rpm) | -0.100 | 5.0 | 16 |
| Hydrothermal | N-doped mesoporous carbon spheres (0.4 $mg_{cat}$ $cm^{-2}$) | 0.1M KOH (at 1600 rpm) | -0.200 | 3.0 | 17 |
| SP | F-doped carbon nanoparticles (0.2 $mg_{cat}$ $cm^{-2}$) | 0.1M KOH (at 10 $mVs^{-1}$and 1600 rpm) | -0.220 | 2.8 | 7 |
| Pyrolysis | F-doped carbon blacks (0.39 $mg_{cat}$ $cm^{-2}$) | 0.1M KOH (at 5 $mVs^{-1}$and 1600 rpm) | -0.158 | 6.1 | 14 |
| SP | B-doped carbon nanoparticles (0.4 $mg_{cat}$ $cm^{-2}$) | 0.1M KOH (at 10 $mVs^{-1}$and 1600 rpm) | -0.180 | 3.2 | 8 |
| CVD | B-doped carbon nanotube | 1M NaOH (at 10 $mVs^{-1}$and 2500 rpm) | -0.350 | 8.0 | 13 |
| SP | B-doped carbon nanoparticles (0.2 $mg_{cat}$ $cm^{-2}$) | 0.1M KOH (at 10 $mVs^{-1}$and 1500 rpm) | -0.250 | 2.7 | This work |
| SP | B/F-doped carbon nanoparticles (0.2 $mg_{cat}$ $cm^{-2}$) | 0.1M KOH (at 10 $mVs^{-1}$and 1500 rpm) | -0.245 | 2.7 | This work |
| SP | B/F-doped carbon nanoparticles (0.2 $mg_{cat}$ $cm^{-2}$) | 0.1M KOH (at 10 $mVs^{-1}$and 2500 rpm) | -0.235 | 3.5 | This work |

that, the mixtures were poured into the SP reactor (**Fig. 1**) and the plasma was generated by a bipolar pulsed power supply (Kurita Seisakusho Co. Ltd.), which provided voltage at 1.5 kV to a pair of tungsten-wire electrodes with a diameter of 1 mm (purity 99.9%, Nilaco Corp.) for 20 min. The optimum pulse width and frequency were 0.5 μs and 100 kHz, respectively. Then, the carbon samples were collected by suction filtration and then washed with pure water, ethanol, and acetone, subsequently. The carbon samples were further dried in an oven at 100 °C for 12 h. For comparison, undoped carbon was also synthesized using toluene alone by the corresponding procedure.

### 2.3 Characterizations

Morphologies of the obtained products from toluene alone and toluene mixed with TPBO, TFPB, TDFPB, and TTFPB via SP were observed by field emission scanning electron microscopy (FE-SEM; JEOL JSM-7610F microscope) at a magnification of ×10000 and ×200000 at an accelerating voltage of 20 kV, and transmission electron microscopy (TEM, a JEOL JEM-2500SE microscope). The specific surface area was investigated by employing the nitrogen absorption-desorption method (BET, Brunauer Emmett Teller) performed on a TriStar- Ⅱ 3020 analyzer equipped with VacPrep 061LB at 77 K. The carbon samples were firstly degassed at 100 °C for 12 h under a vacuum before the measurements. The specific surface area was determined by the Brunauer–Emmett–Teller (BET) method in the relative pressure ($P/P_0$) range of 0.05–0.30. The phase structures were identified by using the X-ray diffractometer (XRD; Rigaku Ultima IV X-ray diffractometer) with monochromatic Cu Kα radiation (λ = 0.154 nm) operating at 40 kV and 40 mA (1.6 kW). Raman spectrometer (JASCO NRS-5100 spectrometer) was used to record the Raman spectra of the obtained carbon samples with a laser-excitation wavelength of 532.11 nm. Elemental analysis was carried out on the CHN analyzer (Perkin Elmer 2400 Series II). X-ray photoelectron spectroscopy (XPS; JEOL JPS-9010MC spectrometer) was used to study the chemical bonding state. The XPS spectrometer with monochromatic Mg Kα radiation (1253.6 eV) as an excitation source under ultra-high vacuum conditions. The operating emission current and anode voltages were 25 mA and 10 kV, respectively.

### 2.4 Electrochemical measurements

A suspension of 5.0 mg the carbon samples in 480 μL ultrapure water, 480 μL ethanol, and 40 μL Nafion® aqueous solution was sonicated until a homogeneous dispersion was obtained (5 mg $mL^{-1}$). 7.5 μL of homogeneous suspension was applied onto a glassy carbon disk (GC) of a rotating-ring disk electrode (RRDE) and allowed to dry in air. Electrochemical measurements for cyclic voltammogram (CVs) and linear sweep voltammograms (LSVs) were carried out on a computer-controlled ALS-CH instrument electrochemical analyzer model 704ES (BAS, Co.) equipped with a rotating ring disk electrode rotator apparatus (RRDE-3A, ALS Co.) and used 0.1 M KOH as the electrolyte. A Pt wire and an Ag/AgCl (KCl sat.) electrode were used as the counter and reference electrodes, respectively. All the experiments were performed at room temperature. Moreover, $N_2$ gas was flowed for 20 min to remove the dissolved $O_2$, gas before the measurements. Then, $O_2$ gas was flowed for 20 min to estimate the electrocatalytic activity of the ORR. The $O_2$ gas was passed on the solution level in the electrochemical cell during the measurements.

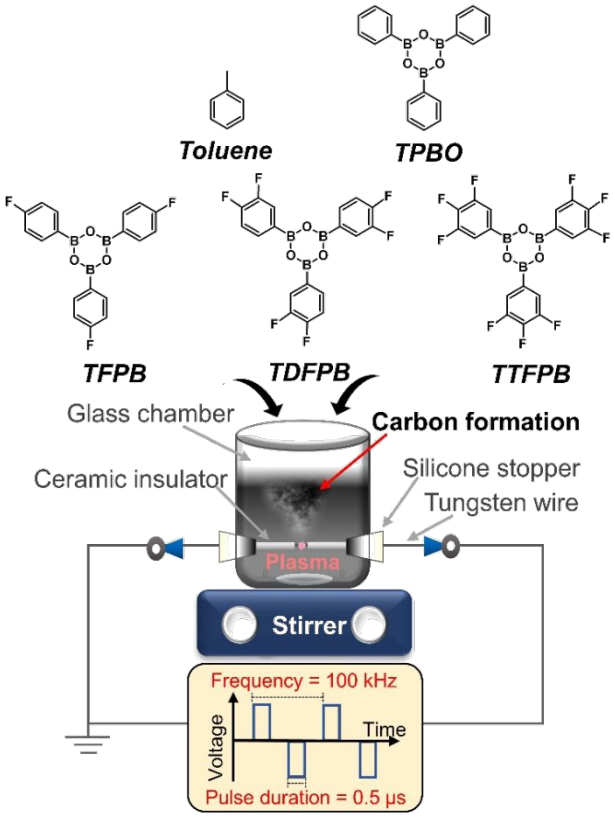


**Fig. 1.** Illustration of the SP setup for synthesis of undoped, boron-doped, and boron/fluorine dual-doped carbon nanoparticles from toluene, toluene mixed TPBO, TFPB, TDFPB and TTFPB.

## 3. Results and discussion

During the SP, some black solid contents were continuously produced as prolonging the plasma treatment time, as schematically illustrated in **Fig. 1**. According to the previous researches, the black particles, which produced directly from plasma zone through the decomposition and recombination of molecules of aromatic hydrocarbons were reported to be carbon materials.[7, 21] Therefore, it could be suggested that the generated black contents via the SP, in this work, could be considered as carbon materials. 2,4,6-triphenylboroxin, 2,4,6-tris(4-fluorophenyl)boroxin, 2,4,6-tris(3,4-difluorophenyl)boroxin and 2,4,6-tris(3,4,5-trifluorophenyl)boroxin were assigned as TPBO, TFPB, TDFPB and TTFPB, respectively. The FE-SEM images of the obtained carbon samples (**Fig. 2**) shows the agglomeration of carbon nanoparticles with a size of approximately 20–40 nm.

To further investigate the textural properties of the obtained carbon samples, the $N_2$ adsorption-desorption analysis using the BET method was used to determine the specific surface area ($S_{BET}$). The $S_{BET}$ of catalyst support can refer to its porosity and pore size distribution, which can have a catalytic site on the surface.[22] Therefore, catalyst performance can be related to the $S_{BET}$ of catalyst

support. The BET adsorption-desorption isotherm and pore size desorption curves, and $S_{BET}$ values of the obtained carbon samples in this work are presented in **Fig. 3** and **Table 2**, respectively. BET adsorption-desorption isotherm curves of all obtained samples were similar. Meanwhile, their pore size distribution exhibited a slight variation. The pore size became smaller and their distribution seemed to become narrower, for the obtained carbons from toluene and toluene with the addition of TPBO, TFPB, TDFPB, and TTFPB via SP, orderly. Therefore, it could be suggested that the presence of fluorine atom in the carbon framework might affect the pore formation. The $S_{BET}$ values were also calculated and found to be slightly varied according to the addition of TPBO, TFPB, TDFPB, and

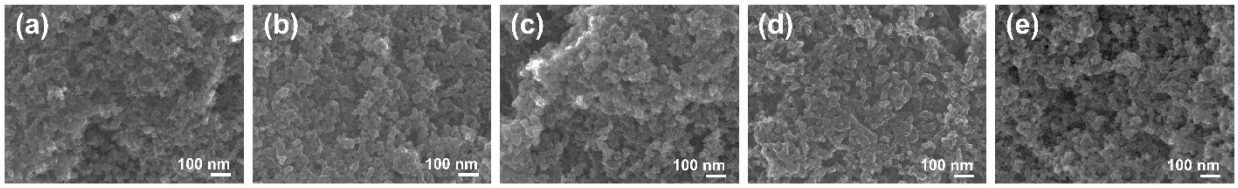


**Fig. 2.** FE-SEM images of the obtained products from (a) toluene, and toluene mixed with (b) TPBO, (c) TFPB, (d) TDFPB, and (e) TTFPB via SP.

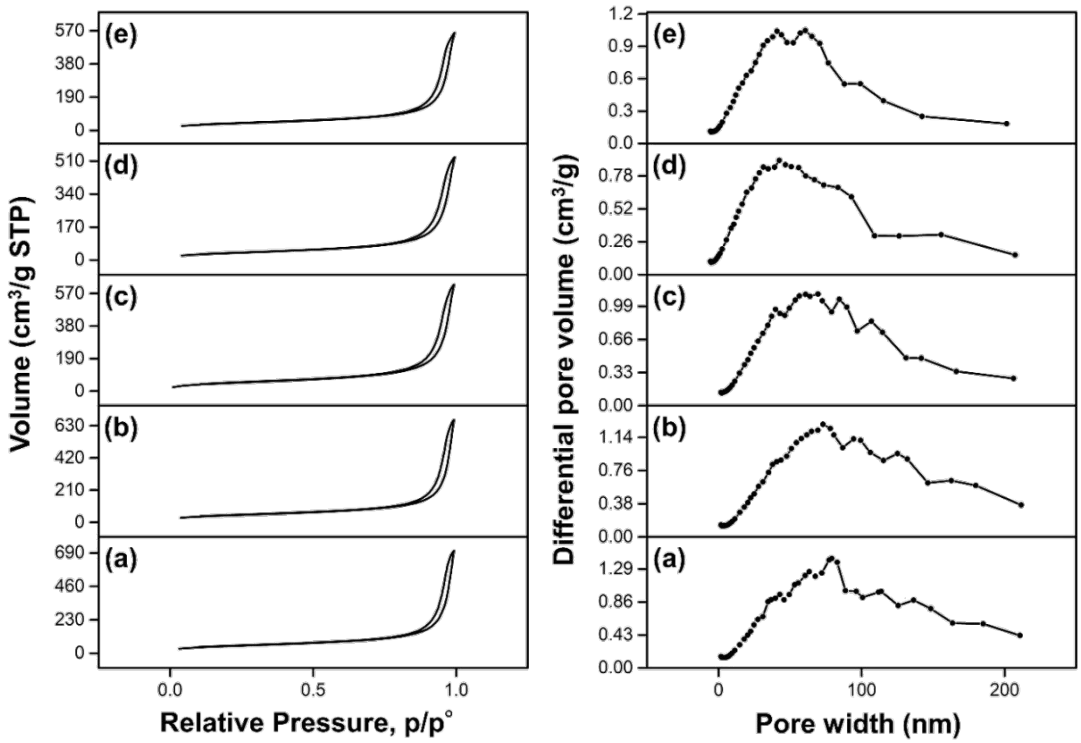


**Fig. 3** BET adsorption-desorption isotherm and pore size curves for the obtained carbons from (a) toluene alone and toluene with the addition of (b) TPBO, (c) TFPB, (d) TDFPB, and (e) TTFPB via SP.

**Table 2** Specific surface area ($S_{BET}$), intensity ratio of D and G bands ($I_D/I_G$) from Raman spectroscopy, bulk element compositions from CHN element analysis (EA) and surface element compositions from XPS measurement of the obtained carbons from toluene alone and toluene with the addition of TPBO, TFPB, TDFPB and TTFPB via SP

| | | | EA (wt%) | | XPS Composition (at%) | | | | Doping concentration* | | |
|---|---|---|---|---|---|---|---|---|---|---|---|
| | $S_{BET}$ ($m^2g^{-1}$) | $I_D/I_G$ | C | H | C | O | B | F | O/C | B/C | F/C |
| Toluene | 177 | 0.885 | 90.9 | 1.28 | 83.1 | 16.9 | - | - | 20.3 | - | - |
| TPBO | 164 | 0.921 | 92.7 | 1.16 | 83.6 | 16.4 | - | - | 19.6 | - | - |
| TFPB | 171 | 0.904 | 91.7 | 1.18 | 90.2 | 9.85 | - | - | 10.9 | - | - |
| TDFPB | 131 | 0.884 | 88.2 | 1.25 | 88.5 | 8.59 | 0.91 | 1.95 | 9.7 | 1.0 | 2.2 |
| TTFPB | 140 | 0.923 | 84.1 | 1.04 | 87.6 | 7.91 | 1.08 | 3.38 | 9.0 | 1.2 | 3.9 |

(Note: wt% means weight percent and at% means atomic percent. *Doping concentration = atomic ratio×100)

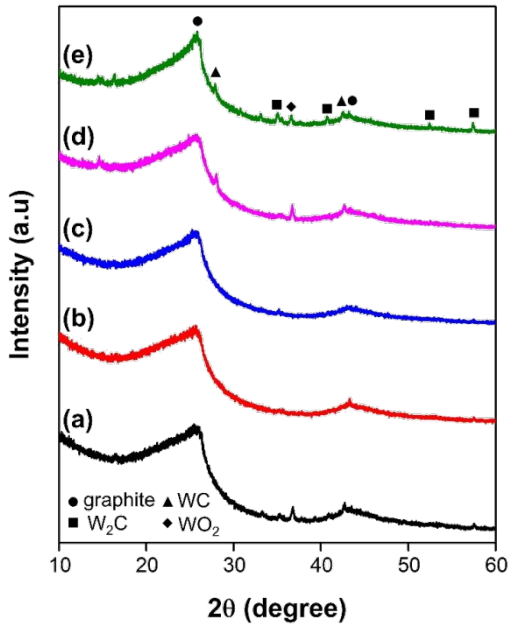


**Fig. 4** XRD patterns of the obtained products from (a) toluene alone and toluene with the addition of (b) TPBO, (c) TFPB, (d) TDFPB, and (e) TTFPB via SP.

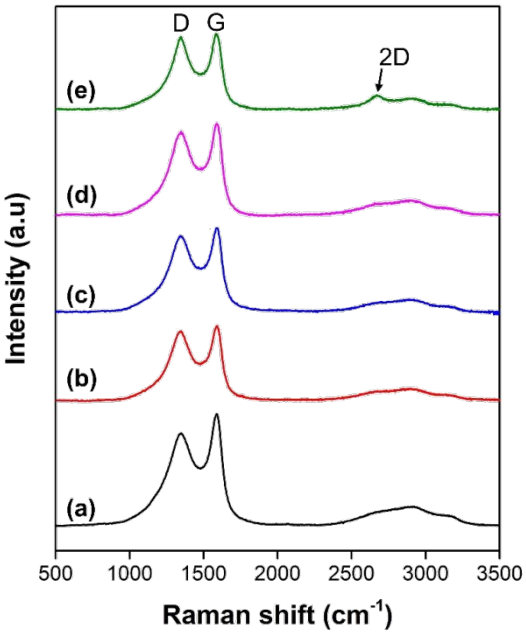


**Fig. 5** Raman spectra of the obtained products from (a) toluene alone and toluene with the addition of (b) TPBO, (c) TFPB, (d) TDFPB, and (e) TTFPB via SP.

TTFPB, which have different chemical structures, including the contents of fluorine atoms, into toluene. The carbon sample from toluene alone exhibited 177 $m^2 g^{-1}$ of $S_{BET}$, but after the addition of TPBO and TFPB, the $S_{BET}$ slightly decreased to 164 and 171 $m^2 g^{-1}$, respectively, while the addition of TDFPB and TTFPB resulted in the decrement of $S_{BET}$ to less than 140 $m^2 g^{-1}$. Accordingly, it could imply that the carbon framework might become more compact due to the partial collapses of pore structures at higher fluorine doping contents, which have been previously reported.[7]

Structural details of the obtained products from toluene alone and toluene with the addition of TPBO, TFPB, TDFPB, and TTFPB via SP were further investigated by XRD and Raman measurements. The XRD pattern of all obtained carbon samples shows a similar pattern with a broad peak at 2θ = 25.5° and weaker peak at 2θ = 43°, which correspond to the 002 and 100/ 101 reflections of turbostratic carbon phase, respectively (**Fig. 4**). This result agreed with the TEM result, as shown in supplementary data Fig. S1. The sharper peaks appeared and shifted toward a lower 2θ angle for the obtained carbon samples from toluene with the addition of TFPB, TDFPB, and TTFPB, compared to that from toluene alone. This result indicated that the doping of boron/fluorine might help to rearrange and develop the ordered stacking of the carbon structure with the expansion of interplanar spacing (d = nλ /2sinθ; n is a number of reflection and λ is wavelength.). However, there were some additional peaks in the XRD pattern of the obtained carbon samples from toluene with the addition of TDFPB, and TTFPB, which belonged to tungsten-based products generated from the tungsten electrodes during the reaction via SP.[19, 23] The similar phenomena was also reported in the previous study which investigated the synthesis of tungsten carbides on N-doped carbon prepared by the erosion of tungsten electrodes via SP.[19] The tungsten carbides including tungsten rich carbide ($W_2C$) and carbon rich carbide (WC) were evaluated and found that the WC on N-doped carbon and the mixture of $W_2C$ and WC on Pt/C could enhance the ORR activity, compared to the original materials without tungsten carbides.[19, 24] Meanwhile, tungsten dioxide ($WO_2$) was reported that its oxygen vacancy could provide a coordination unsaturated sites to adsorb and reduce $O_2$ to super oxides radicals ($O_2^{\bullet-}$) and couple with $H^+$ to form $^{\bullet}OOH$, which may be a competing reaction.[25] Therefore, the ORR activity of samples with the presence of $WO_2$ could be suppressed. Further structural information was analyzed using Raman spectroscopy. Raman analysis is a useful tool for providing detailed information about the structure of graphitic materials.[9] Raman spectra of all obtained carbon samples are revealed in **Fig. 5**. Two conspicuous peaks appeared for all obtained carbon samples at approximately 1352–1390 $cm^{-1}$ and 1585–1590 $cm^{-1}$, associating with D-band and G-band, respectively.[7] The D-band originates from the lattice distortion in the $sp^2$-hybridized carbon or the presence of structural defects, while the G-band is related to $E_{2g}$ phonon mode of the symmetry of the graphite crystal planes.[7, 26] Therefore, the relative intensity ratio of D-band and G-band ($I_D/I_G$) is typically employed as an indicator to determine the degree of graphitization or defect density in carbon materials.[7, 26] The $I_D/I_G$ ratios of the obtained carbon samples were estimated, as shown in **Table 2**. Furthermore, the $I_D/I_G$ values can be used to determine the in-plane crystallite size, $L_a$, using the Tuinstra–Koenig relation, as shown in supplementary data equation S1. The values of $L_a$ are consistent with the inter-defect distance on the surface of the graphene sheet.[9, 27] The calculated $L_a$ values of the obtained carbon samples from toluene and toluene with the addition of TPBO, TFPB, TDFPB, and TTFPB were found to be 21.7, 20.8, 21.3, 21.8 and 21.1 nm. As the

result of Raman measurement, the carbon samples obtained from toluene with the addition of TPBO showed the relatively high value of $I_D/I_G$, indicating the high amount of defect sites. Meanwhile, the carbon samples obtained from toluene with the addition of TFPB and TDFPB revealed small changes in the values of $I_D/I_G$, compared to that obtained from toluene. It could suggest that the boron doping alone could cause high amount of defect sites in the carbon structure than the boron/fluorine dual doping. The possible reason might be that the fluorine atoms that existed on the carbon structure possibly help to rearrange and form the ordered structure, which was also consistent with the XRD results. Though, high fluorine content could also cause high density of defect sites in carbon matrix, as obtained from the Raman result of carbon sample obtained from toluene with the addition of TTFPB. In addition, it was also reported that the attachment of functional groups does not only affected the density of defect sites but also the shape of the defect hole, which also influences the intensity of D-band.[28] According to the BET and Raman results, they could imply that the different amount and positions of fluorine atoms in TFPB, TDFPB, and TTFPB, as shown in **Fig. 1**, were found to result in the different surface area and density of defect sites, which are one of the key factors for facilitating the oxygen transfer and promote the ORR.[7] When fluorine atoms was presented at each phenyl ring of the compound, it was possible that fluorine atoms could form intermolecular interaction with another fluorine atoms in nearby molecule (–C–F…F–C–).[29] For TFPB containing one fluorine atom at each phenyl ring, the –C–F…F–C– interaction might not be formed well, compared to TDFPB, therefore, it seemed to lead to higher defect sites and specific surface area. When the influences of TDFPB and TTFPB were compared, the addition of TTFPB showed much higher surface area and defect sites. It was possible that two fluorine atoms at each phenyl ring of TDFPB might form intermolecular interaction in a planar manner, which help to rearrange the crystalline structure, leading to the graphitic phase. Meanwhile, three fluorine atoms at each phenyl ring of TTFPB might competitively and randomly interact with more two different molecules of TTFPB, resulting in the disordered structure and high defect sites.

Elemental compositions at both bulk and surface of the obtained carbon samples were further investigated by elemental analysis (EA) and XPS spectroscopy, respectively (**Table 2**). The EA results revealed that the elemental compositions in carbon bulk had no significant changes when the boron and fluorine dopants were added. The slight decrease in hydrogen contents was observed in the obtained carbon samples from toluene with the addition of TPBO, TFPB, and TTFPB compared that from toluene alone. The reduction of hydrogen might be occurred by the hydrogen abstraction ability of the generated dopant ions.[7] For the XPS measurement, the surface elemental compositions and chemical bonding states of the obtained carbon samples could be investigated. The surface chemistry of the catalyst is one of the important parameters because the ORR reaction generally occurs at the surface of catalysts.[30] The results of XPS quantitative analysis could confirm the presence of boron and fluorine contents in the obtained carbon products from toluene with the addition of TDFPB and TTFPB via SP. The doping concentrations were also calculated and revealed that the doping concentration of boron remained similar for the obtained carbon products from toluene with the addition of TDFPB and TTFPB, due to the constantly remained amount of boron atoms in both TDFPB and TTFPB. Meanwhile, the doping concentrations of fluorine increased as the number of fluorine atoms increased for TDFPB and TTFPB, respectively, as shown in **Fig. 1**. However, for other obtained carbon samples from toluene with the addition of TPBO and TFPB, the boron and fluorine contents might be lower than the detectable limit, thus, the content values could not be showed. Moreover, to understand the changes of chemical bonding on the surface, the high-resolution XPS spectra were collected with peak deconvolution, as shown in **Fig. 6** and supplementary data Fig. S2. The detailed information of the bonding contents was given in **Table 3**. The major peaks in all obtained carbon samples are the peaks at 285 ± 0.1 eV, contributing to the $sp^2$-hybridized carbon bonding configuration, which is most pronounced for carbon materials.[31] Meanwhile, the evidence regarding the existence of interlayer $sp^3$ carbon bonding between graphene layers, which contained defects such as vacancies and interstitials, was found at a peak of 285.4 ± 0.2 eV.[7, 32] The content of $sp^3$-hybridized carbon bonding slightly increased when the TPBO was added, but gradually decreased with the addition of TFPB, TDFPB, and TTFPB, respectively, compared to that obtained from toluene alone. The result was quite consistent with the result from Raman measurement, which could imply that the doping of boron alone could cause the defect in the carbon structure more than that obtained from the boron/fluorine dual doping. Moreover, there was an additional peak with weak intensity at 289.2 eV appeared for the obtained carbon samples from toluene with the addition of TDFPB and TTFPB. The peak was related to the formation of semi-ionic C-F bonds, which were reported that it could result in a positive influence on the ORR activity of carbon.[7] Toluene with the addition of TTFPB could produce carbon with a higher content of semi-ionic C-F bonds than that produced from the addition of TDFPB. Furthermore, the significant increase of quinone and carbonyl (C=O) groups, from less than 5 at% to approximately 14.5 at% was found from the obtained carbon samples from toluene with the addition of TTFPB. Due to high fluorine content in TTFPB, it was possible to generate fluorine ions via SP, which might draw hydrogen atoms from the existing CO-H on the carbon surface, resulting in C=O. For the high-resolution XPS B 1s (**Fig. 6(a)** and **Fig. 6(c)**), the obtained spectra of both carbon samples from toluene with the addition of TDFPB and TTFPB contained three deconvoluted peaks at 191.0, 192.3 and 193.0 eV, attributing to $BC_2O$, $BCO_2$, and $B_2O_3$, respectively.[8] The presence of the boron oxides might be caused by the oxidation during the SP treatment, which agreed with the previous study.[8] The F 1s spectra of the obtained carbon samples from toluene with the addition of TDFPB and TTFPB were also collected (**Fig. 6(b)** and **Fig. 6(d)**). The most obvious peak centered at 687.5 eV, along with two weak peaks at 685.9 and 690.0 eV, corresponding to ionic, semi-ionic, and covalent C-F, respectively.[7] The result suggested that the obtained carbon samples from toluene with the addition of TDFPB and TTFPB had the semi-ionic characteristic, which can play an important role as electron acceptors, promoting conductivity by facilitating charge

**Table 3** Bonding contents, analyzed from XPS measurement, of the obtained carbon samples from toluene and toluene with the addition of TPBO, TFPB, TDFPB and TTFPB via SP

| | C 1s (%) | | | | | | | B 1s (%) | | | F 1s (%) | | |
|---|---|---|---|---|---|---|---|---|---|---|---|---|---|
| | $sp^2$-C | $sp^3$-C | C-O | C=O | O-C=O | π-π* | Semi-ionic C-F | $BC_2O$ | $BCO_2$ | $B_2O_3$ | Ionic C-F | Semi-ionic C-F | Covalent C-F |
| Toluene | 44.5 | 39.3 | 8.29 | 4.51 | 3.10 | 0.24 | - | - | - | - | - | - | - |
| TPBO | 41.1 | 39.5 | 13.3 | 2.11 | 3.10 | 0.94 | - | - | - | - | - | - | - |
| TFPB | 44.2 | 32.1 | 17.3 | 3.48 | 1.18 | 1.83 | - | - | - | - | - | - | - |
| TDFPB | 48.6 | 28.7 | 16.7 | 0.93 | 2.26 | 1.38 | 1.41 | 14.5 | 49.3 | 36.2 | 2.14 | 86.0 | 11.8 |
| TTFPB | 38.8 | 25.9 | 15.1 | 14.5 | 0.56 | 3.67 | 1.53 | 18.5 | 35.0 | 46.5 | 1.86 | 97.8 | 0.34 |

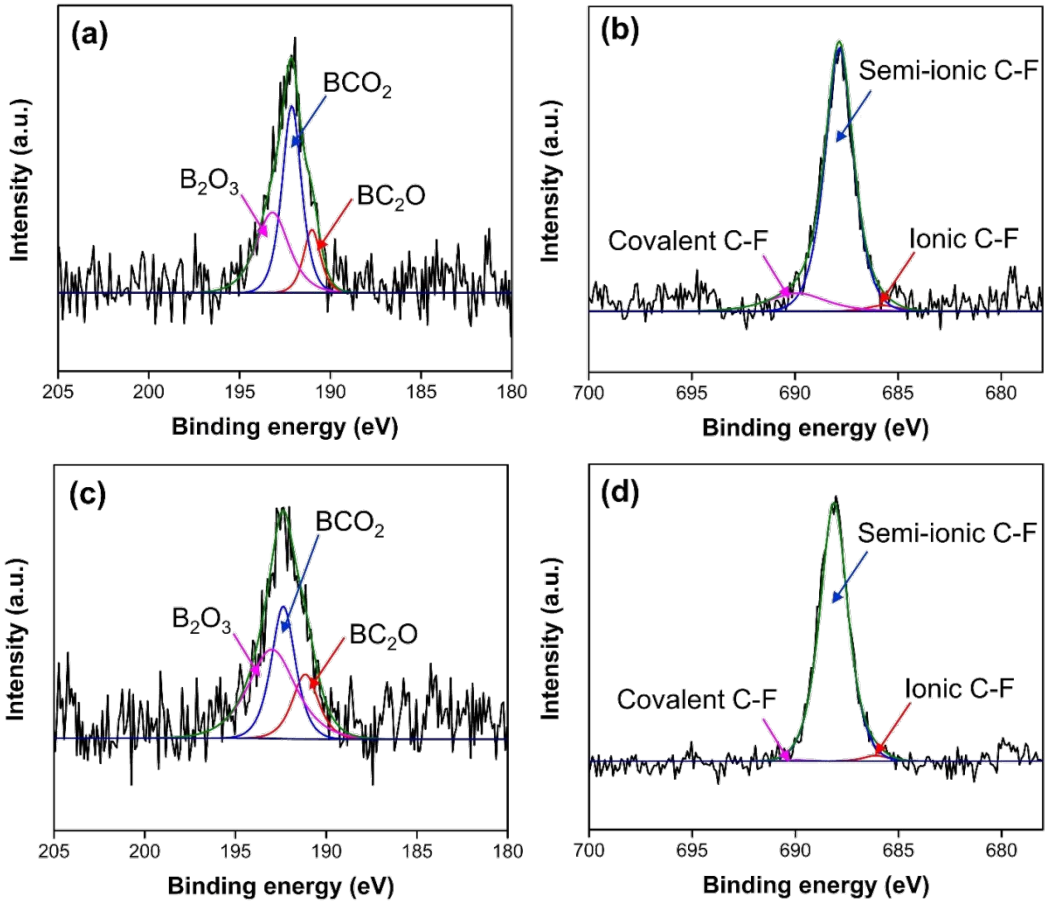


**Fig. 6** High-resolution XPS B 1s spectra of the obtained products from toluene with the addition of (a) TDFPB and (c) TTFPB via SP, and High-resolution F 1s spectra of the obtained products from toluene with the addition of (b) TDFPB and (d) TTFPB via SP.

transfer between fluorine and carbon.[7] Moreover, the semi-ionic bonds were also found to be increased when the higher contents of fluorine were presented.

To study the effect of boron and fluorine dopants on the ORR activity, cyclic voltammetry (CV) measurements of the obtained carbon samples from toluene with the addition of TPBO, TFPB, TDFPB, and TTFPB were conducted, in comparison of that obtained from toluene alone. The CV measurements were performed in 0.1 M KOH solutions saturated with $N_2$ and $O_2$ and recorded in the potential range from -1.0 to 0.2 V (**Fig. 7(a)**). The featureless voltammetric currents in the $N_2$-saturated solution were presented, while the CV curves in the $O_2$-saturated solution exhibited well-defined peak potentials, which referred to the electrochemical activity toward ORR. The peak potentials appeared for all samples at around -0.32–-0.30 V with no significant shifts. To gain further insight into the ORR performance, linear sweep voltammetry (LSV) measurements on an RRDE were conducted in $O_2$-saturated 0.1 M KOH solution at various rotation speeds (supplementary data Fig. S3). **Fig. 7(b)** shows the LSV results of all carbon samples obtained in this work at a rotation speed of 2500 rpm. The disk currents of all carbon samples revealed limiting

current plateaus with further decline. The onset potentials of the obtained carbon samples from toluene and toluene with the addition of TPBO, TFPB, TDFPB, and TTFPB were -0.232, -0.234, -0.233, -0.230 and -0.235 V, respectively. The current densities of all obtained carbon samples from toluene and toluene with the addition of TPBO, TFPB, TDFPB and TTFPB at -0.6 V were found to be 3.5, 3.6, 3.4, 3.6 and 3.5 mA $cm^{-2}$, which were quite comparable to the previous study on the boron-doped carbon synthesized by SP and other methods, as shown in Table 1.

Generally, in the alkaline solution, the ORR can proceed in two different major pathways depending on catalysts, as shown in supplementary data equation S2–S4.[8, 33] The first pathway is known as a direct four-electron pathway, which is the reaction that $O_2$ can directly convert to $OH^-$. The second pathway is a two-electron pathway which is composed of two steps of reduction. At first, $O_2$ is reduced to generate $HO_2^-$ at a low negative potential, and then the absorbed $HO_2^-$ can be further reduced $OH^-$ at a high negative potential. The generated intermediate $HO_2^-$ is unstable and can lead to the production of $H_2O_2$.[26] To indicate the pathway of the ORR, the electron transfer numbers (*n*) were calculated by Koutecky-Levich (K-L) equation based on the LSV curves under different rotating rate (supplementary data equation S5–S6). The K–L plots of $J^{-1}$ versus $\omega^{-1/2}$ of all samples show a linear trend in potentials ranging from –1.0 and –0.3 V (supplementary data Fig. S4). The parallel characteristics of linear fitting lines are shown in the potentials between –0.7 and –0.5 V, indicating a first-order ORR kinetics with respect to oxygen.[8] The *n* values calculated from the slope of the K–L plots are in the range between 2.00 and 2.70 with no obvious change with increasing fluorine doping content over the potential range between –1.0 and –0.3 V (supplementary data Fig. S5). The values of *n* at the potential of –0.6 V were 2.02, 2.02, 2.12, 2.00, 2.00, referring to the two-electron pathway. Moreover, the values of *n* were also confirmed, as well as, amounts of $HO_2^-$ were calculated on the basis of the disk and ring current using the equations shown in supplementary data equation S7–S8.[8, 34] The *n* was calculated from the potential range of from –1.0 to –0.3 V, as shown in **Fig. 8**. As a result, they could be divided into two major groups. One group, including the carbon samples obtained from toluene and toluene with the addition of TPBO and TPFB, had a low range of *n* (2.42–2.80) with high range of $HO_2^-$ yield (60–78%), while the carbon samples obtained from toluene with the addition of TDPFB and TTPFB which contained relative higher fluorine content than others, had a higher range of *n* (2.78–3.00) with the lower range of $HO_2^-$ yield (50–61%). Although the pieces of evidence suggested that the obtained carbons in this study could reduce $O_2$ through the two-electron pathway, the boron/fluorine dual-doped carbon materials showed an approaching to four-electron pathway compared to that obtained from undoped or boron-doped carbons. However, the SP-induced carbon samples obtained from toluene and toluene with the addition of TPBO and TPFB, i.e., undoped and boron-doped carbons, respectively, have the relatively high selectivity toward the generation of $HO_2^-$, which possibly convert to $H_2O_2$. The result was similar to the previous study relating to undoped and boron-doped carbons, which was also prepared by SP using benzene and triphenyl borate.[8] This may open the development of a new system using SP-synthesized carbon-based catalysts for water treatment that can simultaneously generate electricity and degrade organic substances in a chemical waste solution, leading to a solution for energy and pollution crisis.

According to the above results, the electrocatalytic activity of carbons for the ORR could be varied by different starting chemicals.

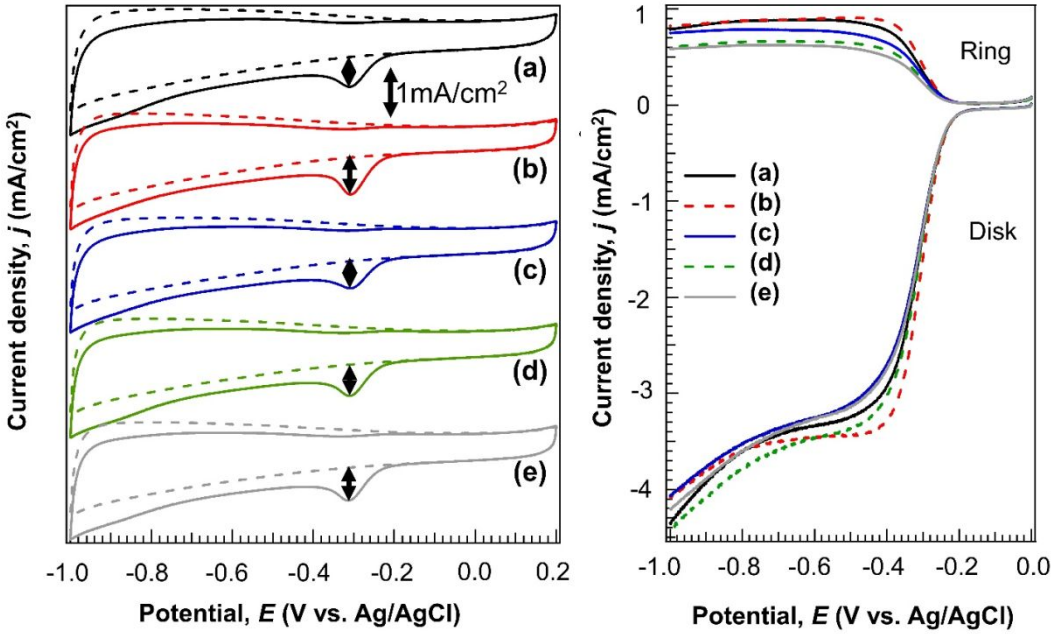


**Fig. 7** Electrochemical measurements: (Right) CV of the obtained products, from (a) toluene, (b) TPBO, (c) TFPB, (d) TDFPB, and (e) TTFPB via SP, in $N_2$ (dash line) and $O_2$-saturated 0.1 M KOH solution at a scan rate of 50 mV $s^{-1}$. (Left) LSV curves of the obtained products, from (a) toluene, (b) TPBO, (c) TFPB, (d) TDFPB and (e) TTFPB via SP, on RRDE in an $O_2$-saturated 0.1 M KOH solution at a scan rate of 10 mV $s^{-1}$ and a rotation speed of 2500 rpm.

In this work, the mixture of toluene with different heterocyclic compounds containing boron and a different amount of fluorine. Among all samples, the doping of boron alone showed the most positive influence on the ORR activity. The boron-doped carbon was previously reported that the presence of boron in carbon structure could cause the electropositive defect sites, due to the electronegativity difference between boron and carbon atoms.[8] When boron atoms with lower electronegativity (2.04 kJ/mol) than that of carbon (2.55 kJ/mol) are presented in the carbon framework, electropositive defect sites can be induced. When both boron and fluorine were simultaneously doped onto the carbon structure, the electrocatalytic activity toward ORR had no significant change. However, they showed higher values of *n* and lowered the generation of $HO_2^-$, which revealed the potential of the ORR approaching the four-electron pathway if further study and development are conducted. It is known that fluorine is the element that has the highest electronegativity (3.98 kJ/mol), resulting in a high ability to attract electrons towards itself. Doping of fluorine atoms into a carbon framework significantly can lead to positive polarization of the neighboring atoms.[35] Once both boron and fluorine atoms are dual-doped, the presence of fluorine atoms should help to induce to the much stronger electropositive defect sites on the carbon framework. The stronger electropositive defect sites should enhance the absorption of $O_2$ and result in the promotion of ORR activity through the direct four-electron pathway, which may be similar to the synergetic effect of graphene dual-doped with boron and nitrogen, which has electronegativity (3.04 kJ/mol) higher than boron.[36] It was also reported that dual doping could create a unique electronic structure between heteroatoms by changing the distribution of electron density.[36, 37] Consequently, dual-doped carbon catalysts should be much more catalytically active than singly doped carbon catalysts. As mentioned before, specific surface area and density of defect sites also play an important role in the ORR activity of carbon-based catalysts. High surface area and density of defect sites was found to provide more active sites for the activation of $O_2$ molecules and facilitate mass diffusion which could also relate to the selectivity of the $HO_2^-$ production.[38] As the result of BET, boron/fluorine dual doped carbon nanoparticles, obtained from the system of TDFPB and TTFPB, showed the low surface area, compared to undoped and boron-doped carbon. The low surface area could reduce the mass diffusion in the carbon matrix, causing the suppression of $HO_2^-$ production.[38] In summary, the possible reasons that boron/fluorine dual doped carbon nanoparticles had the low generation of the $HO_2^-$, compared to undoped and boron-doped carbon, might be having the ORR approaching the four-electron pathway and the suppression of mass diffusion. Therefore, further exclusive investigate on the dual doping of boron/fluorine in the carbon matrix relating to the generation of $HO_2^-$ may lead to the propose of new metal-free carbon as cathodic catalyst in fuel cell application.

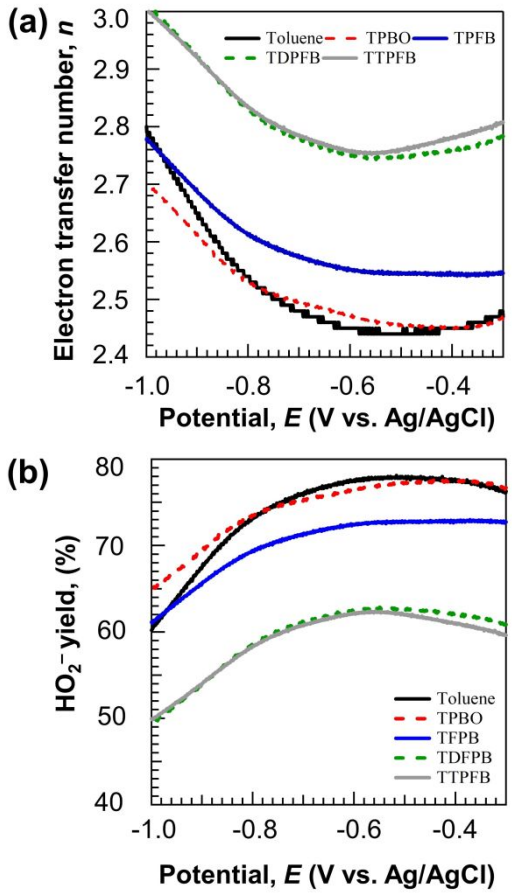


**Fig. 8** (a) Electron transfer number (*n*) values and (b) $HO_2^-$yields of the obtained products**,** from toluene, TPBO, TFPB, TDFPB, and TTFPB via SP, at the potential range from -1.0 to -0.3 V.

## 4. Conclusions

In conclusion, both boron/fluorine-dual doped carbon nanoparticles were successfully synthesized in one pot via SP using the toluene with the addition of TDFPB and TTFPB, and compared with undoped and boron-doped carbon nanoparticles obtained from toluene alone and toluene mixed with TPBO. The boron and fluorine doping resulted in the slight change in the physical properties of the obtained carbon samples, but the presence of boron and fluorine atoms in the carbon framework influenced their ORR. The dual doping of boron and fluorine atoms seemed to lower the amount of the generated $HO_2^-$, therefore, its further development and study may lead to the promising carbon catalyst which can facilitate the ORR through the direct four-electron pathway. Even though, the undoped and boron-doped carbon nanoparticles in this study drove the ORR in the two-electron pathway with the relatively high selectivity toward the generation of $HO_2^-$, this may open a new opportunity for new research. The generation of the unstable $HO_2^-$, which can convert to $H_2O_2$, may be able to apply to invent a new system that can be utilized for water treatment through the oxidation process and simultaneous electricity generation, which may be able to overcome the energy and pollution crisis in the future.

## Conflicts of interest

There are no conflicts to declare.

## Acknowledgments

The authors would like to acknowledge for the financial support, Grant-in-Aid for Scientific Research (B) (No. 19H02482) from Japan Society for the Promotion of Science, Japan Science and Technology Agency (JST) under Program on Open Innovation Platform with Enterprises, Research Institute and Academia (OPERA) (No. 18072116) and JST, Strategic International Collaborative Research Program (SICORP), grant Number JPMJSC18H1, Japan.

## References

1. L. Yang, J. Shui, L. Du, Y. Shao, J. Liu, L. Dai and Z. Hu, *Advanced Materials*, 2019, **31**, 1804799.
2. S. M. Haile, *Acta Materialia*, 2003, **51**, 5981-6000.
3. M.-k. Min, J. Cho, K. Cho and H. Kim, *Electrochimica Acta*, 2000, **45**, 4211-4217.
4. D. Ganguly, R. Sundara and K. Ramanujam, *ACS Omega*, 2018, **3**, 13609-13620.
5. J. Liang, Y. Jiao, M. Jaroniec and S. Z. Qiao, *Angewandte Chemie International Edition*, 2012, **51**, 11496-11500.
6. Q. Lv, W. Si, J. He, L. Sun, C. Zhang, N. Wang, Z. Yang, X. Li, X. Wang, W. Deng, Y. Long, C. Huang and Y. Li, *Nature Communications*, 2018, **9**, 3376.
7. G. Panomsuwan, N. Saito and T. Ishizaki, *Journal of Materials Chemistry A*, 2015, **3**, 9972-9981.
8. G. Panomsuwan, N. Saito and T. Ishizaki, *Electrochemistry Communications*, 2015, **59**, 81-85.
9. T. Ishizaki, S. Chiba, Y. Kaneko and G. Panomsuwan, *Journal of Materials Chemistry A*, 2014, **2**, 10589-10598.
10. K. Preuss, A. M. Siwoniku, C. I. Bucur and M.-M. Titirici, *ChemPlusChem*, 2019, **84**, 457-464.
11. W. Wang, P. Wang, Y. Kang, J. Zhao, P. Tao and Z. Lei, *International Journal of Hydrogen Energy*, 2019, **44**, 4771-4779.
12. Q. Ren, H. Wang, X.-F. Lu, Y.-X. Tong and G.-R. Li, *Advanced Science*, 2018, **5**, 1700515.
13. L. Yang, S. Jiang, Y. Zhao, L. Zhu, S. Chen, X. Wang, Q. Wu, J. Ma, Y. Ma and Z. Hu, *Angewandte Chemie International Edition*, 2011, **50**, 7132-7135.
14. X. Sun, Y. Zhang, P. Song, J. Pan, L. Zhuang, W. Xu and W. Xing, *ACS Catalysis*, 2013, **3**, 1726-1729.
15. S. Jiang, Y. Sun, H. Dai, J. Hu, P. Ni, Y. Wang, Z. Li and Z. Li, *Nanoscale*, 2015, **7**, 10584-10589.
16. G. Panomsuwan, N. Saito and T. Ishizaki, *Physical Chemistry Chemical Physics*, 2015, **17**, 6227-6232.
17. T. Yang, J. Liu, R. Zhou, Z. Chen, H. Xu, S. Z. Qiao and M. J. Monteiro, *Journal of Materials Chemistry A*, 2014, **2**, 18139-18146.
18. T. Morishita, T. Ueno, G. Panomsuwan, J. Hieda, A. Yoshida, M. A. Bratescu and N. Saito, *Scientific Reports*, 2016, **6**, 36880.
19. D.-w. Kim, O. L. Li, P. Pootawang and N. Saito, *RSC Advances*, 2014, **4**, 16813-16819.
20. C. Chokradjaroen, S. Theeramunkong, H. Yui, N. Saito and R. Rujiravanit, *Carbohydrate Polymers*, 2018, **201**, 20-30.
21. D.-w. Kim, O. L. Li and N. Saito, *Physical Chemistry Chemical Physics*, 2015, **17**, 407-413.
22. M. Xu, D. Li, Y. Yan, T. Guo, H. Pang and H. Xue, *RSC Advances*, 2017, **7**, 43780-43788.
23. D. Yoon and A. Manthiram, *Energy & Environmental Science*, 2014, **7**, 3069-3076.
24. Y. Sohn, J. Y. Jung and P. Kim, *Korean Journal of Chemical Engineering*, 2017, **34**, 2162-2168.
25. K. Qian, L. Du, X. Zhu, S. Liang, S. Chen, H. Kobayashi, X. Yan, M. Xu, Y. Dai and R. Li, *Journal of Materials Chemistry A*, 2019, **7**, 14592-14601.
26. C. H. Choi, S. H. Park and S. I. Woo, *Journal of Materials Chemistry*, 2012, **22**, 12107-12115.
27. L. G. Cançado, K. Takai, T. Enoki, M. Endo, Y. A. Kim, H. Mizusaki, A. Jorio, L. N. Coelho, R. Magalhães-Paniago and M. A. Pimenta, *Applied Physics Letters*, 2006, **88**, 163106.
28. B. Krauss, P. Nemes-Incze, V. Skakalova, L. P. Biro, K. v. Klitzing and J. H. Smet, *Nano Letters*, 2010, **10**, 4544-4548.
29. R. M. Osuna, V. Hernández, J. T. L. Navarrete, E. D'Oria and J. J. Novoa, *Theoretical Chemistry Accounts*, 2011, **128**, 541-553.
30. H. Zhang, K. Lv, B. Fang, M. C. Forster, R. Dervişoğlu, L. B. Andreas, K. Zhang and S. Chen, *Electrochimica Acta*, 2018, **292**, 942-950.
31. A. Velázquez-Palenzuela, L. Zhang, L. Wang, P. L. Cabot, E. Brillas, K. Tsay and J. Zhang, *The Journal of Physical Chemistry C*, 2011, **115**, 12929-12940.
32. J. Park, W. C. Mitchel, S. Elhamri, L. Grazulis, J. Hoelscher, K. Mahalingam, C. Hwang, S.-K. Mo and J. Lee, *Nature Communications*, 2015, **6**, 5677.
33. G. Panomsuwan, N. Saito and T. Ishizaki, *RSC Advances*, 2016, **6**, 114553-114559.
34. W. Xing, G. Yin and J. Zhang, *Rotating electrode methods and oxygen reduction electrocatalysts*, Elsevier, 2014.
35. D. Yuan, Z. Wei, P. Han, C. Yang, L. Huang, Z. Gu, Y. Ding, J. Ma and G. Zheng, *Journal of Materials Chemistry A*, 2019, **7**, 16979-16983.
36. Y. Zheng, Y. Jiao, L. Ge, M. Jaroniec and S. Z. Qiao, *Angewandte Chemie International Edition*, 2013, **52**, 3110-3116.
37. K. Meng, Q. Liu, Y. Huang and Y. Wang, *Journal of Materials Chemistry A*, 2015, **3**, 6873-6877.
38. K. Zhao, Y. Su, X. Quan, Y. Liu, S. Chen and H. Yu, *Journal of Catalysis*, 2018, **357**, 118-126.

**Graphical abstract**

# Solution plasma synthesis of boron/fluorine dual-doped carbon electrocatalysts for oxygen reduction reaction